Intramolecular photoinduced proton transfer in 2-(2'-hydroxyphenyl)benzazole family: A TD-DFT quantum chemical study

ARTICLE *in* CHEMICAL PHYSICS · NOVEMBER 2014

Impact Factor: 1.65 · DOI: 10.1016/j.chemphys.2014.10.006

3 AUTHORS, INCLUDING:

Hossein Roohi
University of Guilan
74 PUBLICATIONS **427** CITATIONS

Chemical Physics 444 (2014) 66–76

Contents lists available at ScienceDirect

Chemical Physics

journal homepage: www.elsevier.com/locate/chemphys

Intramolecular photoinduced proton transfer in 2-(2′-hydroxyphenyl)benzazole family: A TD-DFT quantum chemical study

Hossein Roohi *, Nafiseh Mohtamedifar, Fahemeh Hejazi

Department of Chemistry, Faculty of Science, University of Guilan, P.O. Box 98135-674, Rasht, Iran

ARTICLE INFO

Article history:
Received 14 May 2014
In final form 1 October 2014
Available online 13 October 2014

Keywords:
HBO
HBI
HBT
ESIPT
PBE1PBE
AIM

ABSTRACT

In this work, intramolecular photoinduced proton transfer in 2-(2′-hydroxyphenyl)benzazole family (**HBO**, **HBI** and **HBT**) was investigated using TD-DFT calculations at PBE1PBE/6-311++G(2d,2p) level of theory. The potential energy surfaces were employed to explore the proton transfer reactions in both states. In contrast to the ground state, photoexcitation from S_0 state to S_1 one encourages the operation of the excited-state intramolecular proton transfer process. Structural parameters, H-bonding energy, absorption and emission bands, vertical excitation and emission energies, oscillator strength, fluorescence rate constant, dipole moment, atomic charges and electron density at critical points were calculated. Molecular orbital analysis shows that vertical $S_0 \rightarrow S_1$ transition in the studied molecules corresponds essentially to the excitation from HOMO (π) to LUMO (π^*). Our calculated results are in good agreement with the experimental observations.

1. Introduction

Intramolecular H-bonded organic chromophores often exhibit the phenomenon excited-state intramolecular proton transfer (ESIPT) together with fluorescence emission at much longer wavelengths than typical fluorescence. Excited-state intramolecular proton transfer (ESIPT) is a photo-induced procedure in which a proton jumps across the intramolecular hydrogen bond (IMHB) from a proton donor group to a proton acceptor was first described by Weller [1]. In recent years, there has been an increasing attention in ESIPT [2–13] because of its wide applications to such systems as UV-light polymer stabilizers, laser dyes, molecular switches, fluorescence sensors, and particularly in biological systems [14–23]. For instance, it is well accepted that the fluorescence ability of the green fluorescent proteins is controlled by the multiple-proton transfer after photoexcitation [24].

Photoisomerization in the IMHB site in aromatic systems has gained particular attention because of its necessary role in the functionality of so-called photostabilizers which are in wide technical use for the protection of organic polymers against degradation by the UV components of sunlight [25]. Several computational papers published in recent years [26–37] have allowed a remarkable advance toward a full understanding of the photoisomerization process, providing the ground for interpreting the quickly growing amount of experimental results [38–40].

In ESIPT mechanism, there are a number of questions that cannot be answered exclusively by experimental means and that call for a detailed theoretical investigation. For example, what is the structure of the S_1/S_0 systems? Why the ESIPT processes occur? What is the origin of ESIPT mechanism? Computational quantum chemical study on relevant model systems is a promising way to reveal the mechanism of the proton transfer through the IMHB process. Recent researches on ESIPT process have addressed quinoline [35,41] and benzylidene [37] derivatives. They have shown that the enol form is stable in the ground state, and conversion from the enol to the keto form occurs very rapidly after excitation.

The 2-(2′-hydroxyaryl)benzoxazole (**HBO**), 2-(2′-hydroxyaryl)benzimidazol (**HBI**) and 2-(2′-hydroxyaryl)benzthiazol (**HBT**) may be a quit interesting series of fluorophores due to their ESIPT property which leads to a major structural reorganization of the molecules upon photoexcitation and large Stokes shifts. The excited-state behavior of **HBO** [42–46], **HBI** [34,43,47] and **HBT** [43,48–52] and their derivatives has attracted much attention. In recent years, we have studied proton transfer reactions in different systems [53–55]. As we know, ESIPT is strongly influenced by the nature of the substituents and their attachment positions, resulting in the shift of absorption and emission peaks. To the best of our knowledge, there are no computational quantum chemical study

* Corresponding author. Tel.: +98 1313243630 35; fax: +98 1313220066.
E-mail address: hroohi@guilan.ac.ir (H. Roohi).

http://dx.doi.org/10.1016/j.chemphys.2014.10.006
0301-0104/

that in detail addresses the ESIPT process in **HBO**, **HBI** and **HBT**, although there are many theoretical results for very similar systems [56–58]. Recently, we have investigated excited state intramolecular proton transfer (ESIPT) in naphthalene-fused analogue of **HBO**, 2-(2′-Hydroxynaphthyl)benzoxazole [59]. In the present study, we have investigated photophysics and photochemistry of **HBX** (X = O, I and T) molecules with particular emphasis on the nature and mechanism of the ESIPT reaction. In addition, H-bonding interaction along the proton transfer between enol– and keto–tautomers of the **HBO**, **HBI** and **HBT** are characterized by quantum theory of atoms in molecules (QTAIM) [60–62] analyses.

2. Computational details

The stationary points on the S_0 and S_1 potential energy surfaces of **HBO**, **HBI** and **HBT** were optimized using DFT methods (PBE1PBE for S_0) and (PBE1PBE-TD for S_1) [63] in conjunction with the 6-311++G(2d,2p) basis set. DFT methods are used as a reliable standard tool for the theoretical treatment of electronic structure and spectroscopic properties of various types of compounds [64]. The PBE1PBE (TD-PBE1PBE) functional has already provided excitation spectra in very good agreement with the available experimental results [64–67,30,68,32,34]. Vibration frequency calculations were performed analytically and numerically for the S_0 and S_1 states, respectively, to obtain vibrational zero point and thermal energies and to validate that the found structures corresponded to the energy-minima or transition states. They confirmed the presence of minima by the absence of imaginary modes and transition states by a single imaginary mode. The calculations were carried out using the GAMESS [69] and GAUUSIAN 03 program packages [70]. Bulk solvent effects on the ground and the excited states have been taken into account by means of the polarizable continuum model (PCM) using the integral equation formalism variant (IEFPCM) and UFF force field (Radii = UFF). The integrated equation formulation PCM (IEF-PCM) method is a generalization of the PCM method that allows one to deal with anisotropic solvents such as liquid crystals, as well as with isotropic solvents [71–75]. IEF-PCM has given good results when applied to aqueous ionic solutions [76]. The values of the dielectric constants for the model solvents Water, DMSO, DMF, Ethanol and Cyclohexane are 78.35, 46.83, 37.22, 24.85 and 2.02, respectively.

The Bader theory was also applied to find and characterize the critical points. Topological properties of bond critical points (BCPs) were calculated at the PBE1PBE/6-311++G(2d,2p) level of theory by using the AIM2000 program package [77].

3. Results and discussions

The equilibrium structures of the stationary points and their changes provided us with the basis to understand how the molecular structure transformed upon photoexcitation and ESIPT. Closed and open structures of **HBO**, **HBI** and **HBT** at the S_0 and S_1 states are given in Fig. 1. The E forms of the three compounds are planar with C_s symmetry. Each of the molecules can exist as enol (denoted S_0-E) and keto tautomeric forms (denoted S_0-K) in the ground state. In the S_1 state, two E and K forms are symbolized as S_1-E and S_1-K, respectively. The keto forms of the **HBO**, **HBI** and **HBT** are also planar with C_s symmetry.

Fig. 2 illustrates the energy diagram of phototautomerization in the **HBO**, **HBI** and **HBT**. Initially, molecules are in ground states S_0-E. Upon photoexcitation, the molecule is vertically excited to the first excited singlet state S_1-E with the energy difference corresponding to the most intensive peak in the absorption spectrum. The proton transfer (PT) reactions at the S_1 state for **HBO** and **HBI** are different from **HBT**. The PT in the **HBO** and **HBI** starts from the Franck–Condon point S_1-E(FC), with the geometry of the S_0-E state; it passes through the S_1-E state with geometric rearrangement from the S_1-E(FC) state by gaining a certain amount of kinetic energy. From S_1-E state, the molecule can undergoes a tautomerization via ESIPT to the excited state S_1-K or emit a photon and return to the S_0-E state. From the S_1-K, the molecule emits a photon and falls to the ground state S_0-K with the energy difference corresponding to the fluorescence spectrum. Finally, S_0-K in the ground state is relaxed to the S_0-E. For **HBT**, we could not locate the stationary point of its S_1-E form. The S_1-E(FC) structure of **HBT** was converted to its tautomeric form during the geometry optimization due to its barrier-less potential energy surface (PES) for ESIPT so that we observed no energy minimum in the region of the S_1-E state, indicating that the ESIPT of **HBT** is a barrier-less, spontaneous, exothermic process. Thus, from S_1-E(FC) state, the molecule directly undergoes a tautomerization via ESIPT to the excited state S_1-K.

3.1. Structural parameters, H-bonding energy and potential energy curves

The selected optimized structural parameters involved in PT reactions are summarized in Table 1. The value of H-bond angle in **HBO**, **HBI** and **HBT** at S_0 state is 147.3°, 148.7° and 148.0°, respectively. The H-bond strength depends on its length and angle and a small deviation from linearity in the bond angle have the marginal effect on H-bond strength. The O–H bond length in the **HBO**, **HBI** and **HBT** is 0.985, 0.993 and 0.988 Å and the N···HO distance is 1.749, 1.688 and 1.711 Å, respectively. Thus, it is predicted that the strength of H-bonding interaction increases on going from **HBO** to **HBT** and **HBI**.

Table 1 lists the estimated H-bond energies, ΔE_{HB}, of the **HBO**, **HBT** and **HBI** computed by comparing the energies of the closed E form (H-bonded) and the open form, the latter is obtained by 180° rotation of the OH around the C–O bond. The H-bonding energies of **HBO**, **HBI** and **HBT** at the S_0-E state are 11.9, 14.6 and 12.8 kcal/mol, in good agreement with the calculated H-bonding distances. At the S_1-E state, these energies for **HBO** and **HBI** are 12.4 and 15.1 kcal/mol, respectively. Comparison of the H-bonding energy of E forms at two states suggests that upon photoexcitation to the FC region, the strength of H-bonding in **HBO** and **HBI** increases.

Fig. 3 illustrates the potential energy curves (PECs) along the proton transfer (PT) pathway at the ground and excited states as a function of the reaction coordinate (RC = d(OH) – d(NH) for **HBO**, **HBI** and **HBT**. In this work, PECs for PT reaction have been constructed according to the "distinguished coordinate approach" i.e. by specifying a reaction coordinate along which energy change is observed for PT reactions [35,78,79]. In our studied molecules, it is the coordinate along which the transfer of proton occurs from O to N, i.e. elongation of the O–H bond length. Apart from constraining the O–H distance, we relaxed all other degrees of freedom without imposing any symmetry constraints during the geometry optimization. The PES at the S_0 state is strongly asymmetric in favor of the O–H···N H-bond. Inspection of the Fig. 3 reveals that at the S_0 state of **HBO**, **HBI** and **HBT**, enol (S_0-E) forms with OH···N H-bonding are the most stable tautomeric forms. There is no a deep minimum on the potential energy surface of the K forms; rather they are repulsive in nature. The repulsive nature of the ground state PE curve outright discards any chance of the ground state intramolecular proton transfer at the S_0 state. Thus, K forms at the related S_0 states are not stable. They are converted to the E form during the optimization.

Owing to the greater proton affinity of nitrogen with respect to oxygen, the simple enaminone and ketohydrazone systems including N–H···O H-bonding are more stable than their iminoenol and

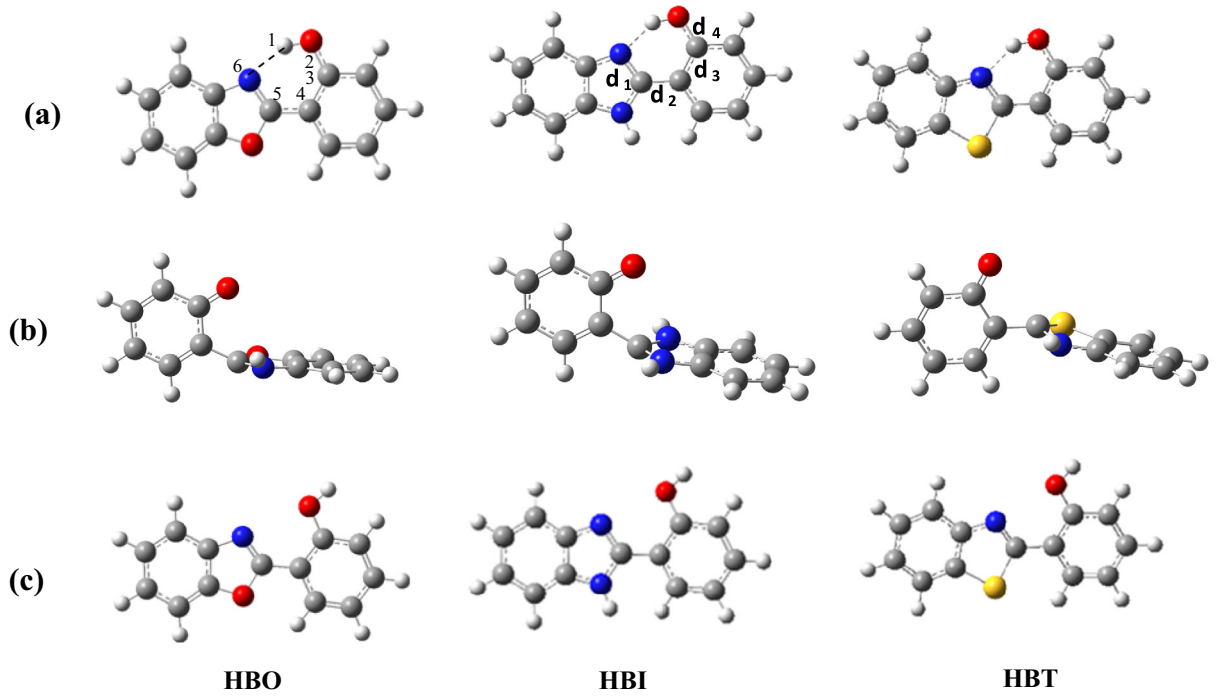

Fig. 1. The closed H-bonded (a), twisted (b) and open non-H-bonded (c) structures of HBO, HBI and HBT.

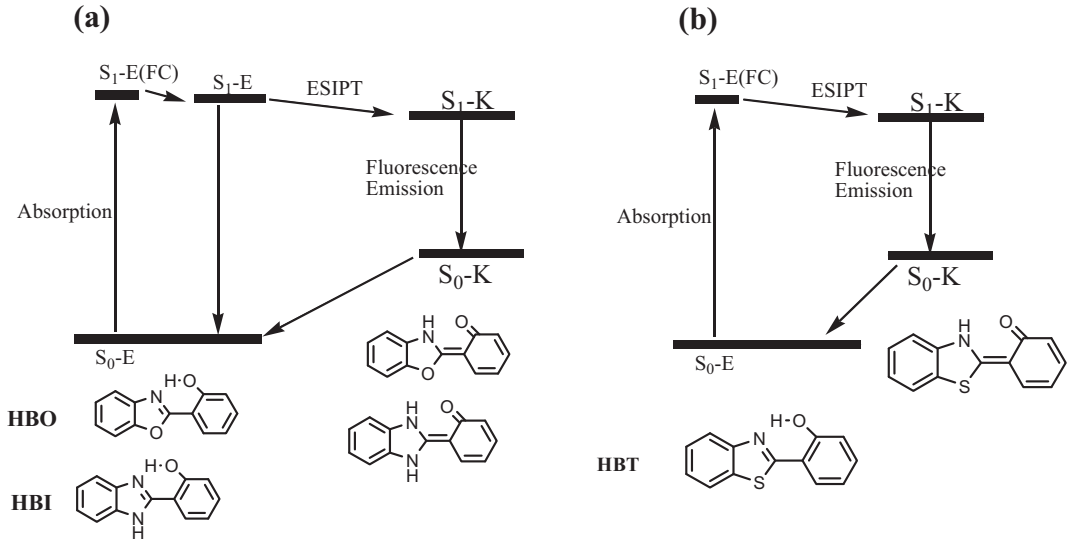

Fig. 2. Energy diagram of phototautomerization for HBO, HBI and HBT.

azoenol ones having O–H···N one [80]. Our results show that the stability order is reversed if a phenyl moiety is fused with the H-bonded ring because the formation of the N–H···O tautomer in the ground state leads to the losing large resonance energy of the benzene ring. Thus, O–H···N tautomer of **HBO**, **HBI** and **HBT** becomes the more-stable tautomer after fusion of the H-bonded ring with a benzene moiety.

The instability of the K forms with respect to the E forms as well as high-energy barrier for E to K transformation (approximately, between 9.0 and 12.5 kcal/mol) on the ground state potential energy surface discards any opportunity of the ground state intramolecular proton transfer (GSIPT) process thermodynamically and kinetically.

Proton transfer in the process of conversion E to K causes the structural changes in the **HBO**, **HBI** and **HBT** at S_0 state. We have examined how the structural parameters are affected by the proton transfer by performing optimization of structures on the potential energy surfaces. Figs. S1 and S2 in the supplementary data show the variations of d(N–H), d(O–H), d(O···N) and O–H···N angle versus RC along the PT pathway of the **HBO**, **HBI** and **HBT** compounds at the S_0 and S_1 states. The PT from O–H···N to O···H–N is associated with the increase of the O–H and decrease of N···H distances. These figures show that the O···N distance first decreases, then passes through a minimum, and finally increases before relaxing to the K form. In addition, variation of O–H···N angle with RC reveals that in contrast to the O···N distance so that it first

Table 1
Selected structural parameters (Å and °) in gas phase and water and H-bonding energies (kcal/mol), ΔE_{HB}, calculated at PBE1PBE/6-311++G(2d,2p) level of theory. Parameters in water are given in parentheses.

	HBO				HBI				HBT		
	S_0-E	S_0-K	S_1-E	S_1-K	S_0-E	S_0-K	S_1-E	S_1-K	S_0-E	S_1-E	S_1-K
O–H	0.985 (0.988)	(1.606)	1.034 (1.001)	1.835 (1.992)	0.993 (0.997)	(1.617)	1.045 (1.011)	1.848 (1.958)	0.988 (0.993)	(1. 019)	1.708 (1.861)
d_1	1.302 (1.302)	(1.325)	1.340 (1.361)	1.340 (1.355)	1.319 (1.323)	(1.350)	1.335 (1.374)	1.350 (1.367)	1.303 (1.304)	(1.362)	1.347 (1.360)
d_2	1.440 (1.441)	(1.407)	1.410 (1.384)	1.433 (1.413)	1.449 (1.451)	(1.425)	1.407 (1.388)	1.444 (1.367)	1.448 (1.450)	(1.396)	1.446 (1.427)
d_3	1.411 (1.411)	(1.445)	1.456 (1.461)	1.433 (1.469)	1.413 (1.412)	(1.443)	1.461 (1.462)	1.457 (1.475)	1.414 (1.413)	(1.465)	1.456 (1.472)
d_4	1.334 (1.340)	(1.277)	1.309 (1.324)	1.269 (1.355)	1.332 (1.339)	(1.281)	1.308 (1.323)	1.268 (1.265)	1.333 (1.338)	(1.317)	1.270 (1.265)
N–O	2.632 (2.622)	(2.494)	2.529 (2.598)	2.609 (2.682)	2.588 (2.570)	(2.505)	2.499 (2.551)	2.615 (2.665)	2.603 (2.587)	(2.540)	2.575 (2.645)
N–H	1.749 (1.732)	(1.057)	1.569 (1.681)	1.027 (1.015)	1.688 (1.659)	(1.051)	1.523 (1.616)	1.022 (1.013)	1.711 (1.687)	(1.596)	1.042 (1.022)
N–H–O	147.28 (147.95)	(138.06)	152.15 (150.25)	129.24 (122.86)	148.65 (149.80)	(138.68)	152.82 (151.53)	129.07 (124.42)	148.03 (148.72)	(151.85)	137.61 (130.78)
ΔE_{HB}	11.9		12.4		14.6		15.1		12.8		

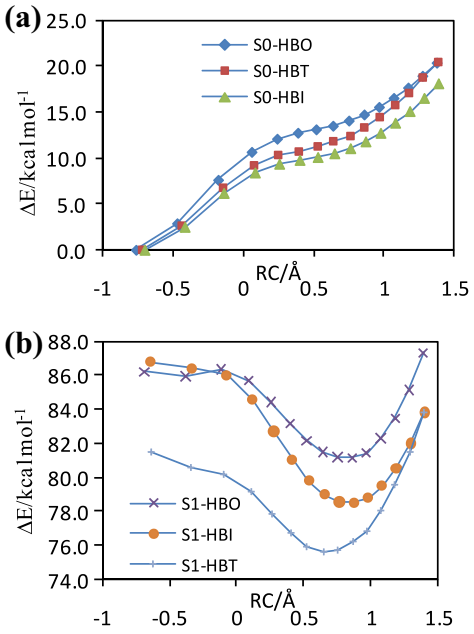

Fig. 3. Potential energy curves along the proton transfer (PT) pathway at the (a) ground and (b) excited states as a function of the reaction coordinate (RC) for HBO, HBI and HBT.

increases, then passes through a maximum, and finally decreases before relaxing to the K form.

The relaxed potential energy curve along the ESIPT pathway at the excited (S_1) states of **HBO**, **HBI** and **HBT** as a function of the reaction coordinate RC = [d(OH) – d(NH)] are depicted in Fig 3b. Apart from constraining the O···H distance, all other degrees of freedom were relaxed without imposing any symmetry constraints during the geometry optimization in S_1 state. Although, it is not clear from Fig. 3b that **HBO** and **HBI** molecules have a minimum at the S_1-E state, but energy of the optimized geometries of **HBO** and **HBI** is, respectively, 4.9 and 4.5 kcal/mol smaller than the corresponding S_1(FC)-E forms. Thus, in the excited (S_1) state, **HBO** and **HBI** shows two planar minima corresponding to the S_1-E and S_1-K forms at the R(O–H) = 1.034 and 1.835 Å for **HBO**, 1.045 and 1.848 Å for the **HBI** and one minimum related to the K form of **HBT** at the 1.708 Å. The R(O–H) of second minimum found in the **HBT** is smaller than others. It should be noted that the E form of **HBT** molecule at S_1 state is converted to K form during geometry optimization using TD-PBE1PBE method.

The S_1-E(FC) states of **HBO**, **HBI** and **HBT** lie at 92.6, 93.1 and 87.9 kcal/mol above the S_0-E, respectively**.** The corresponding energy difference between S_1-K and S_1-E(FC) forms on the PES is −10.8, −12.0 and −9.7 kcal/mol, indicating that the proton transfer at the S_1 state for **HBI** is more exergonic than **HBO** and **HBT**. Although, ESIPT in the S_1 state for **HBT** is barrier-less, there is a barrier separating the S_1-E and S_1-K tautomers of **HBO** and **HBI**. The energy barrier for the conversion S_1-E to S_1-K at the excited state is predicted to be minor. For **HBO** and **HBI** molecules, although barrier heights are small but the existence of these barriers will retard the formation of the S_1-K states and reduce the yields of the S_1-K states. However, access to S_1-K should be facilitated, because the small energy barrier should easily be overcome by the energy gained during the excitation process. Therefore, in contrast to the S_0 ground state, K form of **HBO**, **HBI** and **HBT** can be formed at the S_1 state.

The structural changes upon S_0-E → S_1-E conversion can be analyzed from Table 1. Upon photoexcitation to the first singlet excited state (S_1), the OH group of each molecule becomes more acidic and the nitrogen atom becomes more basic, relative to those in its ground state. The decrease in O···N and H···N distances, increase in O–H bond length and O–H···N bond angle are some structural changes upon photoexcitation in accord with transfer of the proton from OH moiety to the N atom of proton transfer ring at the S_1 state. The other important bond lengths that change upon photoexcitation are d1(C5–N6), d2(C4-C5), d3(C3–C4) and d4(C3-O) bonds in which are defined in Fig. 1. During the S_0-E → S_1-E process, the O–H bond weakens and the H···N H-bond strengthened, causing the d1 and d3 bonds elongated and d2 and d4 ones shortened significantly. The shortening of the central d2 bond during the photoexcitation decreases H···N H-bond, thereby promote the occurrence of the ESIPT process and inhibit the internal rotation of the benzoxazole ring at the S_1 state.

Comparison between the structural parameters of the E with K forms during the ESIPT process reveals how the molecular structures are changed. As illustrated in Fig. 3 the E tautomers are global minima in the S0 state, while they are less stable in the S1 state and are converted to K form during excitation due to their low barrier PES for ESIPT. Thus, E to K tautomerization at the S_1 state can be the main decay channel for **HBO**, **HBI** and **HBT** in the gas phase after the singlet state S_1 is populated.

Figs. S1 and S2 in supplementary data illustrate the variations of d(N–H), d(O–H), d(O···N) and O···H···N angle versus RC along the PT pathway of the **HBO**, **HBI** and **HBT** compounds in the S_1 state. Although plots in Figs. S1 and S2 show similar trends in the variations of d(O···N) distance and O···H···N angle versus RC in the S_0 and S_1 states, but the value of O···N distance is different in the crossover point (COP) of two states. Similar to the S_0 state, O···N distance decreases to a minimum and O···H···N angle increases to a maximum before the transfer of the proton occurs from OH to N atom of benzoxazole ring completely. The COP between E- and K forms of **HBO**, **HBI** and **HBT** lies at RC ≈ 0.061, 0.088 and 0.079 Å, respectively. At the COP, the O···N distance has the lowest amount and it is estimated that the O–H bond character is exchanged with N–H bond character. The O···N distance at the COP of **HBO**, **HBI** and **HBT** is 2.420, 2.413 and 2.418 Å, respectively. Thus, COP in the S_1 state of **HBI** takes place at shorter O···N distance. All of These distortions in the structures take place in order to facilitate the occurrence of the PT reaction in the S_1 state.

3.2. Excitation and emission energies

Since the main focus in the present work is on the ESIPT reaction of **HBO**, **HBI** and **HBT** in the S_1 state, we only discuss the vertical excitation to and emission energies from the lowest excited singlet state (S_1). We have employed time-dependent density functional theory (TD-DFT) to investigate the first singlet excited state behavior of **HBO**, **HBI** and **HBT**.

Upon photoexcitation to the S_1 state, the Franck–Condon excited state, S_1-E(FC), can be relaxed to the minimum of the first excited state S_1-K via ESIPT. In a decay mechanism, K form produced upon ESIPT process is returned to its ground state (S_0-K) accompanied by fluorescence emission and then by a reverse hydrogen transfer in the ground state is converted to S_0-E.

The calculated excitation and emission energies of transitions at PBE1PBE/6-311++G(2d,2p) level in the gas and aqueous phases for optimized S_0-E and S_1-E and S_1-K forms are given in Table 2. The first vertical excitation energies (VEE1) calculated for **HBO**, **HBI** and **HBT** in the gas phase at PBE1PBE/6-311++G(2d,2p) level of theory are 32367 cm^{-1} (309.0 nm), 32521 cm^{-1} (307.5 nm), and 30728 cm^{-1} (325.4 nm), respectively. Accordingly, magnitude of calculated VEE1s is arranged as **HBI** > **HBO** > **HBT**. In other words, VEE1 calculated for **HBI** in the gas phase is greatest and for **HBT** is smallest. Consequently, the energy difference between two electronic levels involved in the transition is lower in **HBT** than others. On the basis of comparison with experimental results, the calculated absorption wavelength of **HBO** (309.0 nm) is comparable with that of the experimental value (335.0 nm in benzene) given in [42].

As recently investigated by Jacquemin et al. [64], TD-DFT is the most widely applied ab initio tool for modeling the electronic spectra and calculation of transition energies of the organic and inorganic molecules and can be extended to incorporate environmental effects either through a modeling of the bulk environment or through a variety of QM/MM approaches. Despite its successes and flexibility, TD-DFT is limited and suffers an important problem: the quality of the obtained results is strongly functional-dependent. With the most favorable functionals, the mean absolute deviations are smaller than 0.25 eV, though the errors significantly depend on the subset of molecules or states considered. Among the TD-DFT functionals, PBE0 provides a mean absolute error of only 0.14 eV for the 228 states related to neutral organic dyes [64].

A red shift in the absorption band is estimated on going from **HBO** to **HBT**, in good agreement with the experimental results obtained for naphthalene-fused benzazole family [42]. The experimental VEE for naphthalene-fused benzazole family is 26500, 28000 and 26800 cm^{-1}, compared with the 32367 cm^{-1} for **HBO**, 32521 cm^{-1} for **HBI** and 30728 cm^{-1} for **HBT**, respectively. Thus, the VEE of our studied molecules is greater than those of obtained for naphthalene-fused benzazole family. Hence, absorption bands of **HBO**, **HBI** and **HBT** in the gas phase are red shifted with respect to those of naphthalene-fused benzazole family, indicating that the insertion of aromatic ring to the **HBO**, **HBI** and **HBT** produces a bathochromic effect on the absorption spectrum of them.

The oscillator strengths, *f*, for $S_0 \rightarrow S_1$ absorption bands of **HBO**, **HBI** and **HBT** appeared at 309.0, 307.5 nm and 325.4 are 0.421, 0.487 and 0.385 respectively. If we compare the position and oscillator strength of the $S_0 \rightarrow S_1$ band of **HBI** with those of **HBO** and **HBT**, we can observe that the intensity of the $S_0 \rightarrow S_1$ absorption band decreases on going from **HBI** to **HBO** and **HBT**.

Fig. S3 in supplementary data shows the variation of the oscillator strength, *f*, of FC transitions versus RC on going from E form to the K one. For **HBO**, **HBI** and **HBT**, it is observed that the *f* value first decreases and then increases on going from **S_1-E** form to **S_1-K** one.

The calculated S_1-K → S_0-K fluorescence emission energy of **HBO**, **HBI** and **HBT** in the gas phase is 63.6 kcal/mol (450.0 nm), 64.7 kcal/mol (442.0 nm) and 60.9 kcal/mol (470.1 nm) at the PBE1PBE/6-31++G(2d,2p) level of theory. The calculated emission energy for **HBO** is in reasonable agreement with the experimentally measured value of 508 nm in the liquid phase [42]. Similar to absorption bands, fluorescence emission wavelength decreases on going from **HBT** to **HBO** and then **HBI**. Therefore, photophysical properties of molecules depend on the substituent inserted on the benzazole ring. Comparison of the *f* values of molecules shows that the intensity of fluorescence emission for **HBO** (0.207) is smaller than **HBI** (0.242) and **HBT** (0.213).

Materials showing high-fluorescence Stokes shifts are used in high-energy radiation detectors. In fluorescent analysis of biological systems, a large Stokes shift is favorable because it corresponds

Table 2
Vertical excitation energies (VEEs), dipole moments, absorption and emission wavelengths (λ1), oscillator strengths (*f*) and fluorescence rate constants (k_f) in the gas phase and water (given in parentheses) at PBE1PBE/6-311++G(2d,2p) level of theory. The S_0-E, S_1-E and S_1-K refers to the optimized geometry used in the vertical excitation energies calculation.

	HBO			HBI			HBT		
	S_0-E	S_1-E	S_1-K	S_0-E	S_1-E	S_1-K	S_0-E	S_1-E	S_1-K
VEE1/cm^{-1}	32366.6 (32324.8)	29036.8 (26673.1)	22223 (22398)	32521.4 (32537.3)	29366.9 (27057)	22622.4 (23182)	30727.6 (30746.5)	(25531)	21273 (21236)
μ/D	2.2 (3.1)	2.2 (2.6)	5.8	3.8 (5.7)	3.8 (5.6)	6.8	2.2 (3.3)	(3.0)	5.6
λ1/nm	309.0 (309.4)	344.4 (374.9)	450.0	307.5 (307.3)	340.5 (369.6)	442.0	325.4 (325.2)	(470.2)	470.1
f1	0.421 (0.600)	0.381 (1.090)	0.207	0.487 (0.665)	0.484 (1.136)	0.243	0.385 (0.539)	(0.214)	0.214
k_f (s^{-1})/10^8			0.683			0.827			0.644

better to the spectral region of less light absorption of biomaterials [81]. All three compounds **HBO**, **HBI** and **HBT** exhibit Stokes-shifted fluorescence. The calculated absorption and emission wavelengths (λ) at PBE1PBE/6-311++G(2d,2p) level of theory are 309.0 and 450.0 nm for **HBO**, 307.5 and 422.0 nm for **HBI** and 325.4 and 470.1 nm for **HBT**, respectively. Therefore, Stokes shift values are 141.0 nm, 114.5 nm and 144.7 nm for **HBO**, **HBI** and **HBT**, respectively. As expected from these values and PE curves given in Fig. 3, Stokes shift for **HBT** is greater than others. The Stokes shifts show that the K form is energetically favored at the S_1 state.

The fluorescence quantum yield is the ratio of photons absorbed to photons emitted through fluorescence. The quantum yield, QY, can also be described by the relative rates of the radiative, k_r, and non-radiative, k_{nr}, relaxation pathways, which deactivate the excited state ($QY = k_r/(k_r + \Sigma k_{nr})$). We have only calculated the fluorescence rate constant, k_f (in s^{-1}), for phototautomeric (S_1-K) forms by using Einstein's emission transition probability equation [82,83]:

$$k_f = f \times \nu(\mathrm{cm}^{-1})/1.5$$

where ν is fluorescence wavenumber and f is the oscillator strength. The calculated fluorescence rate constants are given in Table 2. The calculated k_f values are arranged as **HBI > HBO > HBT** in the gas phase. The radiative lifetime ($\tau = 1/k_f$) of phototautomeric form, S_1-K, of **HBI**, **HBO** and **HBT** molecules were calculated to be 12.1, 14.7, and 15.5 ns in the gas phase, respectively.

3.3. Twisted form of Keto Tautomers at the S_1 state

So far, we have focused on the ESIPT reaction of **HBO**, **HBI** and **HBT** molecules and, in turn, a keto fluorescence emission, while the intramolecular charge-transfer (ICT) reaction [37,42,58,84,85] plays a significant role in the non-fluorescence decay processes in the excited state. The existence of the S_1-ICT forms is particularly important because they quench the fluorescence quantum yield of the S_1-K forms effectively and further influence the excited state photochemical and photophysical behavior. After the excitation of the E from of the S_0 state to the S_1 one, fast ESIPT process occurs to convert the S_1-E to S_1-K. The produced S_1-K can be either relaxed to S_0-K and provides visible fluorescence or converted to the twisted form through ICT reaction.

When the S_1-K-ICT state is preferentially stabilized, the S_1-K → S_1-K-ICT → S_0-K process will be the dominant non-radiative process and the fluorescence quantum yield of the S_1-K state will decreases. It has been suggested that the path via the ICT process, S_1-K → S_1-ICT → S_0-K, is an important non-radiative relaxation process that can reduces the fluorescence quantum yield [37,42,58,84,85].

We found that the **HBO**, **HBI** and **HBT** molecules have both planar S_1-K and twisted S_1-K-ICT configurations. Optimization of the S_1 state of mentioned molecules with C_s symmetry constraint results in a S_1-K planar form. Based on the calculated oscillator strengths, the fluorescence is strongly allowed if it could be observed in the gas phase. An unconstrained optimization of the S_1-K form results in a twisting of the phenolic and benzotriazolic rings as well as in a pyramidalization at the C5 atom.

The Fig. 1b displays the structures of the twisted molecules at S_1 state. For the S_1-K-ICT state of **HBO**, **HBI** and **HBT**, the C3-C4-C5-N6 torsion angles are 69.0°, 71.5° and 101.9°, respectively. The NH···O distance in **HBO**, **HBI** and **HBT** is 3.119, 3.539 and 3.584 Å, respectively. Thus, the twisting breaks the NH···O intramolecular hydrogen bond of S_1-K state and leads to a small pyramidalization at C5 atom.

The energy of the twisted structures of **HBO**, **HBI** and **HBT** in gas phase are smaller than planar C_s ones by 10.1, 8.3 and 13.4 kcal/mol on the potential energy surfaces, indicating that the planar S_1-K conformations are unstable with respect to twisted S_1-K-ICT ones. The energy difference for **HBI** (8.3 kcal/mol) is in good agreement with the results of references [34,56]. The calculated energies for $S_1 \rightarrow S_0$ transition of the twisted molecules of **HBO**, **HBI** and **HBT** are 14.0 (4892 cm^{-1}), 24.8 (8491 cm^{-1}) and 5.0 (1747 cm^{-1}) kcal/mol, respectively, in good agreement with the CASSCF results for the **HBI** [58]. Hence, when the process reaches the S_1-K-ICT state region, its S_1–S_0 energy gap is significantly reduced with respect to the S_1-K state (63.9, 64.7 and 60.9 kcal/mol for **HBO**, **HBI** and **HBT**, respectively) which is effective for internal conversion. Taking into account the formation of S_1-K-ICT species are the effective pathway to quench the fluorescence of S_1-K species, fluorescence ability of the S_1-K state is reduced in order **HBT > HBO > HBI**. Our results for decrease in fluorescence ability of **HBT** is consistent with the findings reported previously using the combining experiments and theoretical calculations [86]. The authors clearly demonstrated that the planar **HBT** at S_1-K state can reaches a nonplanar structural region without a barrier on the S_1 surface in the gas phase. This twisted and pyramidalized structure features an S_0/S_1 conical intersection, which is responsible for ultrafast decay.

3.4. Effect of solvent

Solvent molecules can affect not only the structural equilibrium of species but also their absorption and fluorescence spectra. As mentioned previously, K forms of **HBO**, **HBI** and **HBT** are instable in the gas phase at the S_0 state, whereas those of **HBO** and **HBI** are stable in the aqueous phase and have a minimum on the PES. In contrast, during geometry optimization, similar to the gas phase, K form of **HBT** in the aqueous phase is converted to E form.

The optimized structural parameters for **HBO**, **HBI** and **HBT** in modeled aqueous phase were also given in Table 1. For S_0-E and S_1-K geometries of the **HBO**, **HBI** and **HBT**, the N···H distance decreases and, in turn, O–H distance increases on passing from the gaseous phase to the aqueous one. Besides, NO distance at the S_0-E and S_1-K states decreases and increases, respectively, as the polarity of solvent increases.

The calculated energy difference between S_0-E forms of the gas and aqueous phases ($\Delta E_{gas \rightarrow water}$) is −3.8, −7.1 and −4.1 kcal/mol for **HBO**, **HBI** and **HBT**, respectively, indicating that the stability of E form increases in the polar solvent so that amount of stability for **HBI** is greater than others. The values of ΔE for S_1-E forms of **HBO** and **HBI** are −2.2 and −5.5 kcal/mol and those of the S_1-K forms of **HBO**, **HBI** and **HBT** are −9.3, −13.0 and −9.3 kcal/mol, respectively. Since ΔE for **HBI** is greater than **HBO** and **HBT** in both the S_0 and S_1 states, the stability of **HBI** is more affected than **HBO** and **HBT** by change in the polarity of solvent.

The energy difference between S_1-K and S_1-E(FC) forms on the PES obtained in the aqueous phase is −13.8, −16.5 and −15.0 kcal/mol compared with those obtained in the gas phase (−10.8, −12.0 and −9.7 kcal/mol), indicating that the proton transfer at the S_1 state in the aqueous solution is more exergonic than gas phase. These results also show that the degree of stability of K forms in the aqueous phase is greater than E forms. Thus, due to the larger ΔE for K forms, they are more stabilized than E forms when the polarity of solvent increases.

The results in Table 2 show that the dipole moment of all species increases on going from the gas phase to aqueous phase, indicating that the stability of molecules increases when the polarity of solvent increases. The dipole moment for K form at the S_1 state is greater than E form. Thus, due to the larger dipole moment, the K form can be the dominant form in the polar solvent.

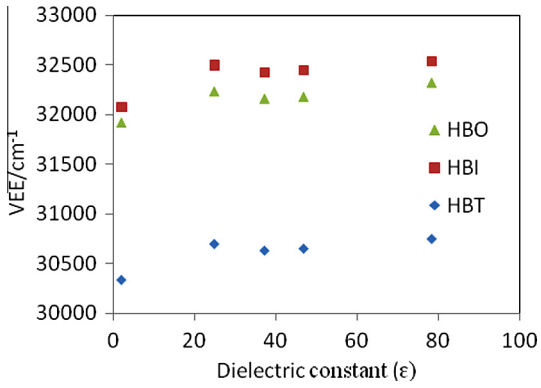

Fig. 4. Correlation between VEE and dielectric constant of different solvent.

Dipole moment for **HBI** in all states and both phases is greater than others, indicating that the considerable charge redistribution is induced by change in substituent. The results reveal that the vertical S_0-E → S_1-E transition leads to decrease of the dipole moment of **HBO** and **HBI** in the aqueous phase without any change in the gas phase. The dipole moment increases on going from S_0-E state to S_1-K state for all molecules in both phases so that this increase in the aqueous phase is greater than gas phase. Accordingly, the E form is slightly more stable in the gas phase, whereas in polar media the K form is predicted to be strongly favored. Besides, S_1-E → S_1-K phototautomerization process in **HBO** and **HBI** leads to a considerable increase in the dipole moment in both phases. Thus, the S_1-K form should be a more stable tautomer in the polar media. As results listed in Table 2 show, increase in polarity of the solvent is accompanied by increase in oscillator strength of the absorption band without any significant shift in their wavelengths.

The effect of solvent on the VEE1 was also investigated in the model nonpolar and polar environments. We have chosen model solvents Ethanol, Water, DMSO, DMF and Cyclohexane. There is a correlation between VEE1 and dielectric constant of solvents. Fig. 4 shows this correlation. The VEE1 increases as the dielectric constant increases from 2.016 (Cyclohexane) to 37.22 (DMF), 46.83 (DMSO) and 78.35 (H_2O). Therefore, the energy difference between S_0 and S_1 states for these solvents increases as the polarity of solvent increases. Hence, the ground state is more stabilized by polar solvent as expected from the solutes dipole moment values. For a given solvent, plot shows that the VEE1 of the compounds is in order **HBI** > **HBO** > **HBT**.

3.5. The Frontier molecular orbital analysis

The excitation from S_0-E to S_1 and in turn redistribution of charge density causes the proton donor OH groups of the studied molecules become more acidic relative to those in its ground state. Our results show that the vertical $S_0 \rightarrow S_1$ transition in the Frank–Condon region of **HBO**, **HBI** and **HBT** molecules corresponds essentially to the excitation from HOMO (π) to LUMO (π^*), which are mostly located in different parts of the molecule (Figs. 5 and S4). In the following, we preferentially focus on the electron density projection over the PT (IMHB) ring. Analysis of the HOMO within IMHB ring reveals that the HOMO in the S_0-E form of all molecules (**HBO**, **HBI** and **HBT**) is a π orbital with bonding character across the OH, d3(C3–C4) and d1(C5–N6) bonds and antibonding character across the d2(C4-C5) and d4(C3-O) bonds.

The LUMO in the E form is a π^* orbital with bonding character centered along the d2 bond axis and antibonding character located along the O–H, d1, d3 and d4 bond axes. After excitation from HOMO to LUMO, the π-bond character of the d1 and d3 bonds decreases and, consequently, the corresponding bond lengths

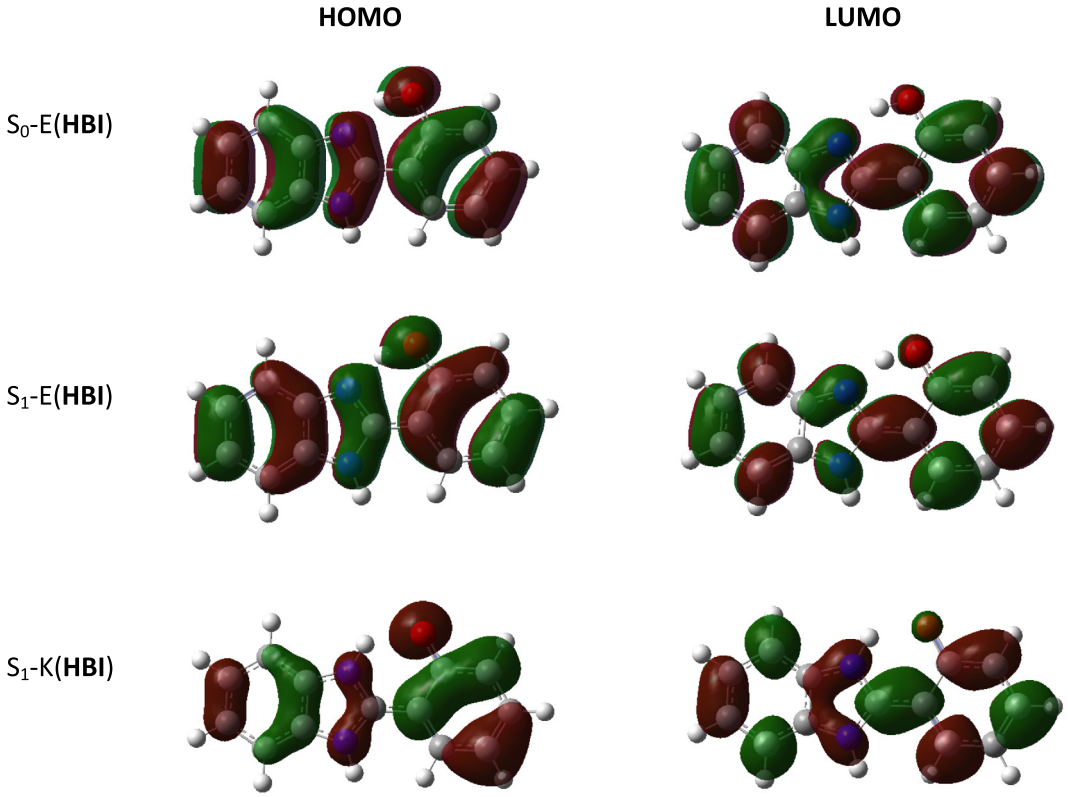

Fig. 5. Frontier HOMO and LUMO molecular orbitals for S_0-E, S_1-E and S_1-K states of HBI.

Table 3
Topological properties of the electron density (au) at PBE1PBE/6-311++G(2d,2p) level of theory.

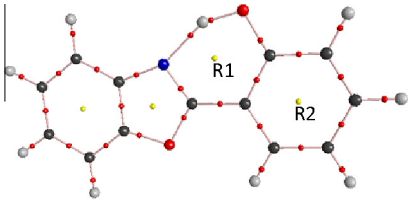

	S_0-E			S_1-E			S_1-K		
	ρ(r)	$\nabla^2\rho(r)$	H(r)	ρ(r)	$\nabla^2\rho(r)$	H(r)	ρ(r)	$\nabla^2\rho(r)$	H(r)
HBO									
O–H	0.3435	−2.5985	−0.7208	0.2975	−2.0500	−0.5854	0.0378	0.1164	−0.0008
N···H	0.0461	0.1097	−0.0062	0.0713	0.1003	−0.0225	0.3223	−2.0258	−0.5514
d_1	0.3786	−1.2705	−0.5592	0.3337	−1.0606	−0.4737	0.3448	−1.1522	−0.4926
d_2	0.2866	−0.7775	−0.2728	0.2763	−0.6978	−0.2610	0.2841	−0.7554	−0.2842
d_3	0.3027	−0.8342	0.3005	0.2791	−0.7078	−0.2523	0.2807	−0.7194	−0.2554
d_4	0.3140	−0.6250	−0.4951	0.3693	−0.7127	−0.6263	0.3708	−0.7238	−0.6294
Ring1(R1)	0.0190	0.1127	0.0042	0.0184	0.1135	0.0043	0.0173	0.1030	0.0038
Ring2(R2)	0.0237	0.1597	0.0058	0.0225	0.1507	0.0057	0.0225	0.1506	0.0058
HBI									
O–H	0.3345	−2.5029	−0.6983	0.2862	−1.9041	−0.5520	0.0367	0.1162	−0.0004
N···H	0.0538	0.1107	−0.0104	0.0805	0.0883	−0.0298	0.3281	−2.0713	−0.5633
d_1	0.3640	−1.1912	−0.5120	0.3381	−1.0170	−0.4235	0.3353	−1.0921	−0.4701
d_2	0.2807	−0.7390	−0.2587	0.3039	−0.8827	−0.3089	0.2773	−0.7156	−0.2664
d_3	0.3019	−0.8291	−0.2986	0.2753	−0.6682	−0.2442	0.2784	−0.7039	−0.2511
d_4	0.3163	−0.6415	−0.5001	0.3335	−0.6121	−0.5435	0.3715	−0.7307	−0.6311
Ring1(R1)	0.0196	0.1188	0.0043	0.0220	0.1371	0.0048	0.0170	0.1005	0.0038
Ring2(R2)	0.0236	0.1594	0.0058	0.0222	0.1500	0.0058	0.0224	0.1504	0.0058
HBT									
O–H	0.3395	−2.5511	−0.7105				0.0497	0.1301	−0.0056
N···H	0.0513	0.1109	−0.0089				0.3102	−1.8863	−0.5195
d_1	0.3698	−1.1854	−0.5577				0.3337	−1.0606	−0.4737
d_2	0.2803	−0.7308	−0.2585				0.2763	−0.6978	−0.2610
d_3	0.3012	−0.8242	−0.2975				0.2791	−0.7078	−0.2523
d_4	0.3152	−0.6299	−0.4980				0.3693	−0.7127	−0.6263
Ring1(R1)	0.0196	0.1177	0.0044				0.0184	0.1135	0.0043
Ring2(R2)	0.0237	0.1594	0.0058				0.0225	0.1507	0.0057

increase. In contrast, the π-bond character of the d2 bond increases. The shortening the d2 bond and, therefore, decreasing the OH···N distance, are favorable for ESIPT. Consequently, HOMO to LUMO transition facilitates proton transfer. In addition, upon electronic excitation from HOMO to LUMO at the S_0-E state, electron density on the O atom decreases. In other words, excitation of the electron leads to depletion of electron density at the O–H bond and, in turn, weakness of this bond. Thus, upon excitation of the electron from HOMO to LUMO in the Franck–Condon region, the hydroxyl proton is expected to be more acidic, which will facilitate or even trigger the subsequent transfer of the proton.

The HOMO of the K form within IMHB ring of all studied molecules is a π orbital composed of bonding contributions mainly along the d1 and d3 bonds axes along with large electron density on the carbonyl oxygen. The antibonding contributions of HOMO are located across d2 and d4 bonds. The LUMO is also a π^* orbital with bonding character centered along the d2 bond axis and antibonding characters located along the d1, d3 and d4 bond axes. Upon electronic excitation from HOMO to LUMO, electron density on the O atom decreases and that of the N atom increases. The presence of antibonding contributions along the d1, d3 and d4 prevents the electron delocalization in the PT ring and thereby forbids the reverse PT from K form to E one at the S_1 state.

3.6. AIM analysis

The quantum theory of atoms in molecules (QTAIM) is a useful tool to characterize hydrogen bonding. One of the advantages of the AIM theory is that one can obtain information on changes in the electron distribution, as a result of either bond formation or complex formation [87,88]. The molecular graphs (including the critical points and bond paths) of the E and K forms of molecules are shown as supplementary data in Fig. S5. In addition to all of the expected BCPs, the electron density analysis reveals an additional BCP in OH···N (E form) and NH···O (K form) distances and a ring critical point in IMHB region.

AIM method can be a great help for assessing the variations in chemical bond nature occurring along the PT pathway. In proper HBs, formation of the Y···H–X H-bond is accompanied by a weakening of the covalent H–X bond with the concomitant decrease of the H–X stretching frequency and decrease of electron density of the H–X bond. The calculated values of electron density, ρ(r), Laplacian of electron density, $\nabla^2\rho(r)$, and electronic energy density, H(r), at the bond and ring critical points at PBE1PBE/6-311++G(2d,2p) level of theory for the ground and excited states are listed in Table 3.

The results show that for **HBO**, **HBI** and **HBT**, ρ(r) value at the N···H BCP is 0.0461, 0.0538 and 0.0513 au and H(r) value is −0.0062, −0.0104 and −0.0089 au, respectively. Hence, H-bond interaction in **HBI** is stronger than **HBO** and **HBT**. Besides, ρ(r) value at the C–O (d4) BCP for **HBI** (0.3163 au) is greater than others. There is a simple interpretation: the stronger the N···HO H-bond is, the more mobile the electron pair of oxygen is and the stronger the d4 bond may be.

Nature of H-bonding interactions can be more clearly understood from the $\nabla^2\rho(r)$ and H(r) values. The results in Table 3 show

a positive value for $\nabla^2\rho(r)$ and slightly negative value for H(r) at the N···H and O···H BCPs. According to the Bader's criteria [60,61], natures of both OH···N and O···HN H-bonds are classified as partial covalency. The values of ρ(r) (0.0538 au) and much more negative value of H(r) (−0.0104) at N···H BCP of **HBI** imply that the covalency nature of the H-bonding in **HBI** is greater than others, in good agreement with a much shorter H-bond distance found for **HBI**. Accordingly, measure of covalency nature of N···H H-bonds is as **HBI** > **HBT** > **HBO**. An increase of H-bond strength (i.e. increasing of the ρ(r) at H-bond CP) is accompanied with a lengthening of the O–H bond and in turn decreasing of ρ(r) at the O–H BCP.

The results in Table 3 reveal that the electron density at the N···H BCP increases upon photoexcitation from S_0-E state to S_1-E state. Thus, this transition facilitates PT at the S_1 state. For **HBI**, increase of electron density (0.0267 au) at the N···H BCP upon photoexcitation from S_0-E state to S_1-E state is greater than **HBO** (0.0252 au).

It is interesting to compare the strength of NH···O H-bonding in the S_1-K form of **HBO**, **HBI** and **HBT**. The value of ρ(r) at NH···O BCP given in Table 3 is 0.0378, 0.0367 and 0.0497 au, indicating that the H-bond interaction in S_1-K form of **HBT** is stronger than the **HBO** and **HBI**. From H(r) values, it can be concluded that covalency nature of NH···O for **HBT** is greater than others. Upon phototautomerization, OH···N interaction is replaced by NH···O one. Comparisons of ρ(r) values suggest that the OH···N interactions in E forms are stronger than NH···O ones in K forms.

Figs. 6 for **HBI** and S6 for **HBO** and **HBT** show the change in the ρ(r) and $\nabla^2\rho(r)$ at the OH···N as well as O–HN bond critical points (BCPs) during the proton transfer reaction at the S_0 state. The sharp variation of the topological parameters (ρ(r) and $\nabla^2\rho(r)$) against the RC, in fact, confirms the presence of strong H-bonding interaction in these compounds. As these Figs. show, the increase in BCP data [ρ(r), and $\nabla^2\rho(r)$] of OH···N bond is accompanied by decrease in those of O–HN one.

The variation of C–C central bond (d2) and the corresponding electron density versus reaction coordinate (RC) along the PT pathway of the **HBO**, **HBI** and **HBT** molecules at the S_0 state are shown in Fig. 7 (top curve). The d2 bond length decreases and electron density increases on going from E form to K one, indicating that the double nature of central C–C bond increases. The magnitude of the decrease in electron density at d2 BCP is different for the studied molecules. Variation of Laplacian of electron density as well as electronic energy density along the PT pathway of the **HBO**, **HBI** and **HBT** at the S_0 state is depicted in Fig. 7 (bottom curve). This figure illustrates that the negative value of Laplacian of electron density as well as electronic energy density increases along the PT pathway.

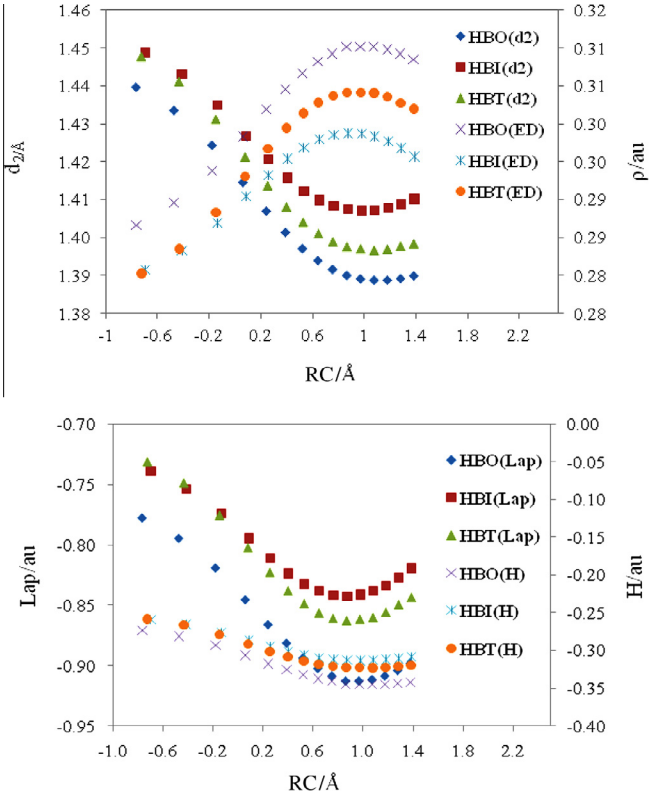

Fig. 7. Variation of electron density (ED) at the d2 BCP as well as d2 bond length versus RC (top) and Laplacian of electron density (Lap) as well as electronic energy density (H) (bottom) along the PT pathway of the HBO, HBI and HBT isomers at the S_0 state.

The formation of the H-bonding in **HBO**, **HBI** and **HBT** closes a 6-membered ring and is accompanied by the appearance of a ring critical point (RCP) in the proton transfer ring (R1). The value of electron density at the RCP can provide the useful information regarding the ring electronic current and understanding the quality of the results. The value of electron density at the RCP of PT ring (R1) for E form of the **HBO**, HBI and HBT molecules is smaller than that of the phenolic ring (R2) linked to R1. Interestingly, values of ρ at the R1 and R2 RCPs for the S_0-E forms are 0.0190 and 0.0237 au for **HBO**, 0.0196 and 0.0236 au for **HBI**, 0.0196 and 0.0237 au for **HBT**, respectively. These values for S_1-E states are 0.0184 and 0.0225 au for **HBO** and 0.0220 and 0.0222 au for **HBI**, respectively (Table 3). The ρ at the R2 decreases upon photoexcitation from

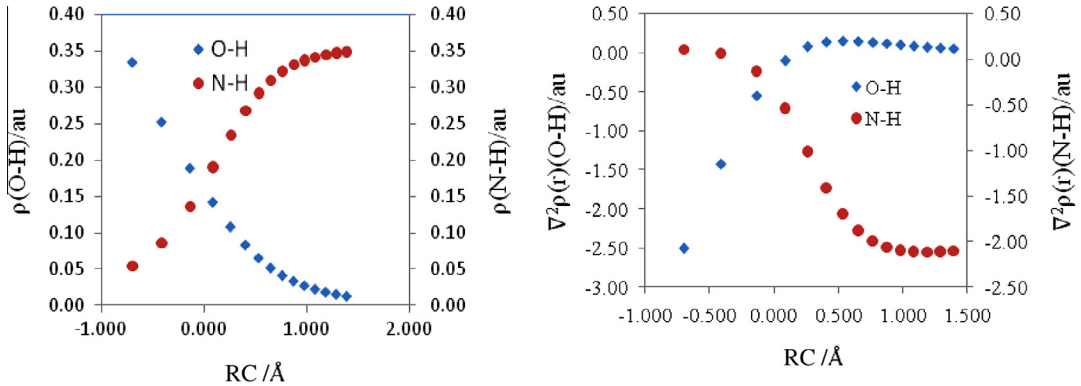

Fig. 6. Variation of electron density and Laplacian of electron density $\nabla^2\rho(r)$ at the N(O)–H BCP versus RC along the PT pathway of the HBI at the S_0 state.

Table 4
AIM population analysis data (in au) calculated at PBE1PBE/6-311++G(2d,2p) level of theory for atoms involved in proton transfer.

	HBO			HBI			HBT	
	S_0-E	S_1-E	S_1-K	S_0-E	S_1-E	S_1-K	S_0-E	S_1-K
q_N	−0.9999	−0.9796	−1.04669	−0.9938	−0.9825	−1.0332	−0.9998	−1.0548
q_H	0.6377	0.5381	0.5381	0.6379	0.6280	0.5303	0.6387	0.5406
q_O	−1.1289	−1.1357	−1.1717	−1.1265	−1.1440	−1.1706	−1.1189	−1.1565

S_0-E state to S_1-E one. Besides, ρ at the R1 of the **HBO** decreases and for **HBI** increases upon this photoexcitation**.**

The occurrence of ESIPT implies that a certain amount of electronic charge is transferred between proton donor and acceptor moieties by photoexcitation. The charge density values calculated at PBE1PBE/6-311++G(2d,2p) level of theory in the gas phase using integration over atomic basins are given in Table 4. For several typical H-bonded systems, it has been demonstrated that the charge is transferred from the proton acceptor to the proton donor [89]. The charge density on the O atom (as a proton donor atom) involved in IMHB of **HBO**, **HBI** and **HBT** in the $S_0(S_1)$ states of the E form is −1.1289 (−1.1357) au, −1.1265 (−1.1440) au and −1.1189 au, respectively, indicating that the charge density of O atom increases upon photoexcitation from S_0 to S_1 one. Upon photoexcitation from S_0-E to S_1-E, the negative charge of N atom and positive charge of H atom in **HBO** and **HBI** decreases. By comparing the charges of the O atoms, it can be seen that the negative charges of the O atoms at the S_0-E state increase in the following sequence: **HBT < HBI < HBO**.

4. Conclusions

Our studies demonstrate the effect of substituents inserted in the benzazole ring on the ESIPT photochemical reaction. For all of the studied compounds, the E forms were calculated to be the dominant ground state species in both the gas and aqueous phases due to their lower energies than the tautomer K forms. The instability of the K forms discards any opportunity of the ground state intramolecular proton transfer (GSIPT) process. But, access to S_1-K in the excited state is facilitated, because the ESIPT reaction for studied molecules is a barrier-less process and is energetically favored. The calculations in the excited (S_1) state showed that the **HBO** and **HBI** have three minima (E, K and ICT forms) on the PES and **HBT** shows two minima (K and ICT forms).

Decrease in O···N and H···N distances, increase in O–H bond length and O–H···N bond angle are some structural changes upon photoexcitation. The results show that the magnitude of calculated VEEs for $S_0 \rightarrow S_1$ transition is: **HBI > HBO > HBT**. The validity of PBE1PBE/6-311++G(2d,2p) level of theory was confirmed in the prediction of the photophysical parameters of **HBO**, **HBI** and **HBT**. A red shift in the absorption band is estimated on going from **HBO** to **HBT**. The fluorescence emission wavelength decreases on going from **HBT** to **HBO** and then **HBI**. All three compounds **HBO**, **HBI** and **HBT** exhibit Stokes-shifted fluorescence so that its value for **HBT** is greater than others. Taking into account the formation of S_1-K-ICT species are the effective pathway to quench the fluorescence of S_1-K species, fluorescence ability of the S_1-K state is reduced in order **HBT > HBO > HBI.**

In contrast to the gas phase, calculations in the aqueous phase show that the K forms of **HBO** and **HBI** are stable in the aqueous phase and have a minimum on the PES of the ground state. The stability of **HBI** is more affected than **HBO** and **HBT** by change in polarity of the solvent. The calculated k_f values in both phases are arranged as **HBI > HBO > HBT**.

Our results show that the vertical $S_0 \rightarrow S_1$ transition in the Frank–Condon region of **HBO**, **HBI** and **HBT** molecules corresponds essentially to the excitation from HOMO (π) to LUMO (π*). By comparing the charges of the O atoms, it can be seen that the negative charges of the O atoms increase in the following sequence **HBT < HBO < HBI**. The results reveal that the charge is transferred from benzazole ring to proton donor one in the both S_0-E and S_1-E states of **HBO** and **HBI**. AIM results show that the measure of covalency nature of N···H H-bonds is in order **HBI > HBT > HBO**. The results reveal that the electron density at the N···H BCP increases upon photoexcitation from S_0-E state to S_1-E state.

Conflict of interest

There is no conflict of interest.

Appendix A. Supplementary data

Supplementary data associated with this article can be found, in the online version, at http://dx.doi.org/10.1016/j.chemphys.2014.10.006.

References

[1] A.H. Weller, Prog. React. Kinet. 1 (1961) 187.
[2] R. Das, A.S. Klymchenko, G. Duportail, Y. Mely, J. Phys. Chem. B 112 (2008) 11929.
[3] A.S. Klymchenko, V.V. Shvadchak, D.A. Yushchenko, N. Jain, Y. Mely, J. Phys. Chem. B 112 (2008) 12050.
[4] C.L. Chen, C.W. Lin, C.C. Hsieh, C.H. Lai, G.H. Lee, C.C. Wang, P.T. Chou, J. Phys. Chem. A 113 (2009) 205.
[5] T. Mutai, H. Tomoda, T. Ohkawa, Y. Yabe, K. Araki, Angew. Chem. Int. Ed. 47 (2008) 9522.
[6] S.G. Roh, Y.H. Kim, K.D. Seo, D.H. Lee, H.K. Kim, Y.I. Park, J.W. Park, J.H. Lee, Adv. Funct. Mater. 19 (2009) 1663.
[7] A. Brenlla, F. Rodriguez-Prieto, M. Mosquera, M.A. Rios, M.C.R. Rodriguez, J. Phys. Chem. A 113 (2009) 56.
[8] J.M. Ortiz-Sanchez, R. Gelabert, M. Moreno, J.M. Lluch, J. Chem. Phys. 129 (2008) 214308.
[9] M. Gauden, A. Pezzella, L. Panzella, M.T. Neves-Petersen, E. Skovsen, S.B. Petersen, K.M. Mullen, A. Napolitano, M. Ischia, V. Sundstrom, J. Am. Chem. Soc. 130 (2008) 17038.
[10] W.H. Sun, S.Y. Li, R. Hu, Y. Qian, S.Q. Wang, G.Q. Yang, J. Phys. Chem. A 113 (2009) 5888.
[11] K.Y. Chen, Y.M. Cheng, C.H. Lai, C.C. Hsu, M.L. Ho, G.H. Lee, P.T. Chou, J. Am. Chem. Soc. 129 (2007) 4534.
[12] P.T. Chou, G.R. Wu, C.Y. Wei, M.Y. Shiao, Y.L. Liu, J. Phys. Chem. A 104 (2000) 8863.
[13] K.-C. Tang, M.-J. Chang, T.-Y. Lin, H.-A. Pan, T.-C. Fang, K.-Y. Chen, W.-Y. Hung, Y.-H. Hsu, P.-T. Chou, J. Am. Chem. Soc. 133 (2011) 17738.
[14] D. Kuila, G. Kvakovszky, M.A. Murphy, R. Vicari, M.H. Rood, K.A. Fritch, J.R. Fritch, S.T. Wellinghoff, S.F. Timmons, Chem. Mater. 11 (1999) 109.
[15] Z. Liang, Z. Liu, L. Jiang, Y. Gao, Tetrahedron Lett. 48 (2007) 1629.
[16] S.J. Lim, J. Seo, S.Y. Park, J. Am. Chem. Soc. 128 (2006) 14542.
[17] B.L. Feringa (Ed.), Molecular Switches, Wiley-VCH, Weinheim, Germany, 2001.
[18] Y. Wu, X. Peng, J. Fan, S. Gao, M. Tian, J. Zhao, S. Sun, J. Org. Chem. 72 (2007) 62.
[19] A. Sytnik, M. Kasha, Proc. Natl. Acad. Sci. U.S.A. 91 (1994) 8627.
[20] Y. Kubo, S. Maeda, S. Tokita, M. Kubo, Nature 382 (1996) 522.
[21] Q.J. Ma, X.B. Zhang, X.H. Zhao, Y.J. Gong, J. Tang, G.L. Shen, R.Q. Yu, Spectrochim. Acta Part A Mol. Biomol. Spectrosc. 73 (2009) 687.
[22] K.I. Sakai, M. Ichikawa, Y. Taniguchi, Chem. Phys. Lett. 420 (2006) 405.
[23] A.L. Sobolewskia, Phys. Chem. Chem. Phys. 10 (2008) 1243.
[24] M. Zimmer, Chem. Rev. 102 (2002) 759.
[25] J. Catalan, J.C. Dell Valle, R.M. Claramunt, D. Saunz, J. Dotor, J. Lumin. 68 (1996) 165.
[26] L. Gagliardi, G. Orlandi, V. Molina, P.A. Malmqvist, B.O. Roos, J. Phys. Chem. A 106 (2002) 7355.
[27] J. Quenneville, T.J. Martinez, J. Phys. Chem. A 107 (2004) 829.
[28] Y. Dou, R.E. Allen, J. Chem. Phys. 119 (2003) 10658.

[29] D.M. Leitner, B. Levine, J. Quenneville, T.J. Martinez, P.G. Wolynes, J. Phys. Chem. A 107 (2003) 10706.
[30] R. Improta, F. Santoro, C. Dietl, E. Papastathopoulos, G. Gerber, Chem. Phys. Lett. 387 (2004) 509.
[31] C. Dietl, E. Papastathopoulos, P. Niklaus, R. Improta, F. Santoro, G. Gerber, Chem. Phys. 310 (2005) 201.
[32] R. Improta, F. Santoro, J. Phys. Chem. A 109 (2005) 10058.
[33] L. Biemann, S.A. Kovalenko, K. Kleinermanns, R. Mahrwald, M. Markert, R. Improta, J. Am. Chem. Soc. 133 (2011) 19664.
[34] H.G. Tsai, H.S. Sun, C. Tan, J. Phys. Chem. A 114 (2010) 4065.
[35] B.K. Paul, N. Guchhait, J. Lumin. 131 (2011) 1918.
[36] K. Sakota, C. Jouvet, C. Dedonder, M. Fujii, H. Sekiya, J. Phys. Chem. A 114 (2010) 11161.
[37] G. Cui, Z. Lan, W. Thiel, J. Am. Chem. Soc. 134 (2012) 1662.
[38] H. Gorner, H.J. Kuhn, Adv. Photochem. 19 (1995) 1.
[39] D. Panda, P.P. Mishra, S. Khatua, A.L. Koner, R.B. Sunoj, A. Datta, J. Phys. Chem. A 110 (2006) 5585.
[40] A. Szemik-Hojniak, I. Deperasinska, L. Jerzykiewicz, P. Sobota, M. Hojniak, A. Puszko, N. Haraszkiewicz, G. van der Zwan, P. Jacques, J. Phys. Chem. A 110 (2006) 10690.
[41] M. Higashi, S. Saito, J. Phys. Chem. Lett. 2 (2011) 2366.
[42] T. Iijima, A. Momotake, Y. Sinohara, T. Sato, J. Phys. Chem. A 114 (2010) 1603 and references cited therein.
[43] S.R. Vazquez, M.C.R. Rodriguez, M. Mosquera, F. Rodriguez-Prieto, J. Phys. Chem. A 111 (2007) 1814.
[44] H. Wang, H. Zhang, O.K. Abou-Zied, C. Yu, F.E. Romesberg, M. Glasbeek, Chem. Phys. Lett. 367 (2003) 599.
[45] T. Arthen-Engeland, T. Bultmann, N.P. Ernsting, M.A. Rodriguez, W. Thiel, Chem. Phys. 163 (1992) 43.
[46] A. Fernandez-Ramos, J. Rodrıguez-Otero, M.A. Rios, J. Soto, J. Mol. Struct. (Theochem) 489 (1999) 255.
[47] F. Rodriguez-Prieto, J.C. Penedo, M.J. Mosquera, Chem. Soc. Faraday Trans. 94 (1998) 2775.
[48] C. Schriever, S. Lochbrunner, R.A. Ofial, E. Riedle, Chem. Phys. Lett. 503 (2011) 61–65 and references cited therein.
[49] O.F. Mohammad, S. Luber, V.S. Batista, E.T.J. Nibbering, J. Phys. Chem. A 115 (2011) 7550.
[50] C. Schriever, M. Barbatti, K. Stock, A.J.A. Aquino, D. Tunega, S. Lochbrunner, E. Riedle, R. Vivie-Riedle, H. Lischka, Chem. Phys. 347 (2008) 446.
[51] J.J. Zheng, Y.X. Guo, X.P. Li, G.L. Zhang, W.J. Chen, J. Optics, Optics 8 (2006) 835.
[52] T. Elsaesser, W. Kaiser, Chem. Phys. Lett. 128 (1986) 231.
[53] H. Roohi, R. Taghezadeh, J. Fluorine Chem. 132 (2011) 459.
[54] H. Roohi, K. Roshan, Struct. Chem. 24 (2013) 1319.
[55] H. Roohi, B. Moghadam, J. Mol. Model. 18 (2012) 1313.
[56] F.A.S. Chipem, N. Dash, G. Krishnamoorthy, J. Chem. Phys. 134 (2011) 104308.
[57] H. Konoshima, S. Nagao, I. Kiyota, K. Amimoto, N. Yamamoto, M. Sekine, M. Nakata, K. Furukawa, H. Sekiya, Phys. Chem. Chem. Phys. 14 (2012) 6448.
[58] F.A.S. Chipem, G. Krishnamoorthy, J. Phys. Chem. A 113 (2009) 12063.
[59] H. Roohi, F. Hejazi, N. Mohtamedifar, M. Jahantab, Spectrochim. Acta Part A Mol. Biomol. Spectrosc. 118 (2014) 228.
[60] R.F.W. Bader, Atoms in Molecules. A Quantum Theory, Clarendon Press, Oxford, UK, 1990.
[61] R.F.W. Bader, H. Essen, J Chem. Phys. 80 (1994) 1943.
[62] R.F.W. Bader, Can. J. Chem. 76 (1998) 973.
[63] C. Adamo, V. Barone, J. Chem. Phys. 110 (1999) 6158.
[64] D. Jacquemin, V. Wathelet, E. Perpete, C. Adamo, J. Chem. Theory Comput. (JCTC) 5 (2009) 2420.
[65] C. Adamo, G.E. Scuseria, V. Barone, J. Chem. Phys. 111 (2000) 2889.
[66] C.A. Guido, D. Jacquemin, C. Adamo, B. Mennucci, J. Phys. Chem. A 114 (2010) 13402.
[67] D. Jacquemin, C. Peltier, I. Ciofini, J. Phys. Chem. A 114 (2010) 9579.
[68] D. Jacquemin, E. Bremond, A. Planchat, I. Ciofini, C. Adamo, J. Chem. Theory Comput. (JCTC) 7 (2011) 1882.
[69] M.W. Schmidt, K.K. Baldridge, J. Boatz, S.T. Elbert, M.S. Gordon, J.H. Jensen, S. Koseki, N. Matsunaga, K.A. Nguyen, S.J. Su, T.L. Windus, M. Dupuis, J.A. Montgomery, J. Comput. Chem. 14 (1993) 1347.
[70] M.J. Frisch, G.W. Trucks, H.B. Schlegel, G.E. Scuseria, M.A. Robb, J.R. Cheeseman, J.A. Montgomery Jr., T. Vreven, K.N. Kudin, J.C. Burant, J.M. Millam, S.S. Iyengar, J. Tomasi, V. Barone, B. Mennucci, M. Cossi, G. Scalmani, N. Rega, G.A. Petersson, H. Nakatsuji, M. Hada, M. Ehara, K. Toyota, R. Fukuda, J. Hasegawa, M. Ishida, T. Nakajima, Y. Honda, O. Kitao, H. Nakai, M. Klene, X. Li, J.E. Knox, H.P. Hratchian, J.B. Cross, V. Bakken, C. Adamo, J. Jaramillo, R. Gomperts, R.E. Stratmann, O. Yazyev, A.J. Austin, R. Cammi, C. Pomelli, J.W. Ochterski, P.Y. Ayala, K. Morokuma, G.A. Voth, P. Salvador, J.J. Dannenberg, V.G. Zakrzewski, S. Dapprich, A.D. Daniels, M.C. Strain, O. Farkas, D.K. Malick, A.D. Rabuck, K. Raghavachari, J.B. Foresman, J.V. Ortiz, Q. Cui, A.G. Baboul, S. Clifford, J. Cioslowski, B.B. Stefanov, G. Liu, A. Liashenko, P. Piskorz, I. Komaromi, R.L. Martin, D.J. Fox, T. Keith, M.A. Al-Laham, C.Y. Peng, A. Nanayakkara, M. Challacombe, P.M.W. Gill, B. Johnson, W. Chen, M.W. Wong, C. Gonzalez, J.A. Pople, Gaussian 03, Revision E.01, Gaussian Inc, Wallingford, CT, 2004.
[71] M. Cossi, N. Rega, M. Scalmani, V. Barone, J. Chem. Phys. 114 (2001) 5691.
[72] B. Mennucci, R. Cammi, J. Tomasi, J. Chem. Phys. 109 (1998) 2798.
[73] E. Cancès, B. Mennucci, J. Tomasi, J. Chem. Phys. 107 (1997) 3032.
[74] G. Scalmani, M.J. Frisch, J. Chem. Phys. 132 (2010) 114110.
[75] J. Tomasi, B. Mennucci, R. Cammi, Chem. Rev. 105 (2005) 2999.
[76] M. Cossi, V. Barone, B. Mennucci, J. Tomasi Chem. Phys. Lett. 286 (1998) 253.
[77] F. Biegler-König, J. Schönbohm, D. Bayles, J. Comput. Chem. 22 (2001) 545.
[78] A.L. Sobolewski, W. Domcke, Chem. Phys. 232 (1998) 257.
[79] S. Prasad De, S. Ash, D.K. Bhui, H. Bar, P. Sarkar, G.P. Sahoo, A. Misra, Spectrochim. Acta Part A 71 (2009) 1735.
[80] P. Gilli, V. Bertolasi, L. Pretto, L. Antonov, G. Gilli, J. Am. Chem. Soc. 127 (2005) 4943.
[81] A.V. Gaenko, A. Devarajan, I.V. Tselinskii, U. Ryde, J. Phys. Chem. A 110 (2006) 7935.
[82] J.M. Hollas, Modern Spectroscopy, John Wiley & Sons Ltd, 1995.
[83] A.J.A. Aquino, H. Lischka, C. Hattig, J. Phys. Chem. A 109 (2005) 3201.
[84] A.L. Sobolewski, W. Domcke, C. Hattig, J. Phys. Chem. A 110 (2006) 6301.
[85] H.-H.G. Tsai, H.-L.S. Sun, C.-J. Tan, J. Phys. Chem. A 114 (2010) 4065.
[86] M. Barbatti, A.J.A. Aquino, H. Lischka, C. Schriever, S. Lochbrunner, E. Riedle, Phys. Chem. Chem. Phys. 11 (2009) 1406.
[87] U. Koch, P.L.A. Popelier, J. Phys. Chem. 99 (1995) 9747.
[88] P.L.A. Popelier, J. Phys. Chem. A 102 (1998) 1873.
[89] A.E. Reed, L.A. Curtiss, F. Weinhold, Chem. Rev. 88 (1988) 899.